Desalination and Water Treatment
www.deswater.com

doi: 10.5004/dwt.2020.25348

188 (2020) 266–276
June

Simultaneous removal of the toxic tungsten ions and rhodamine B dye by graphene nanosheets from model and real water

Salem A. Hameed[a], Mohamed A. Abdel-Fadeel[a,b], Hamed M. Al-Saidi[c], Mohamed Abdel Salam[a,*]

[a]*Chemistry Department, Faculty of Science, King Abdulaziz University, P.O. Box: 80200-Jeddah 21589, Saudi Arabia, email: masalam16@hotmail.com (M.A. Salam), Tel. +966-541886660; Fax: +966-2-6952292; email: drshameed@hotmail.com (S.A. Hameed), Tel. +966-596256654; Fax: +966-2-6952292; email: m_abdelazeem@hotmail.com (M.A. Abdel-Fadeel)*
[b]*Biomedical Laboratory, Chest Hospital, Mansoura, Dakahlia, Egypt*
[c]*Chemistry Department, University College in Al–Jamoum, Umm Al-Qura University, Saudi Arabia, Tel. +966-541886660; Fax: +966-2-6952292; email: hmh1973@hotmail.com (H.M. Al-Saidi)*

Received 13 June 2019; Accepted 13 December 2019

ABSTRACT

This work describes the application of graphene nanosheets (GNS) as a solid adsorbent for the simultaneous removal of the toxic tungsten ions (W^{+6}) and rhodamine B dye (RhB) from model and real water. Physical characterization of the GNS showed their presence as overlapped sheets of different length and width, and with an average thickness of 20.0 nm and a high specific surface area of 279 m^2 g^{-1}. The influence of different experimental conditions on removal efficiency such as pH of the solution, GNS mass, contact time, solution temperature, and ionic strength were investigated. The results from the experimental data showed GNS can remove most of W ions and RhB species from the aqueous solution in 30 min, at pH 1.0, with adsorption efficiency of 99.1% using 17.5 mg of GNS, and with adsorption capacity 93.5 mg of W g^{-1} of GNS and 41.8 mg of RhB g^{-1} of GNS. The removal process of W ions and RhB dye by GNS were studied kinetically using different kinetic models, and the results indicated the pseudo-second-order kinetic model suitability for the adsorption process description. The removal process was studied thermodynamically, and the results revealed that the removal was spontaneous, endothermic in nature, and associated with increase in randomness. Finally, the efficiency of GNS for the adsorption of tungsten ions and rhodamine B dye from real samples were explored using three different real environmental water samples. The data confirms that GNS has great efficiency in removing tungsten ions and rhodamine B dye from aqueous solution.

Keywords: Adsorption; Rhodamine B dye; Tungsten ions; Kinetics; Thermodynamics

1. Introduction

Recently, the interest in tungsten chemistry, occurrences, uses and environmental problems have increased due to its toxicological effects on humans, related to the natural residue of tungsten ore [1–3]. Tungsten, and its alloy and compounds, are important materials in industrial applications such as military, machining, chemical and electronic industry and other, due to its excellent chemical and physical properties [4]. Therefore, the chance for pollution of the environmental samples with this element is very probable. Trace element of tungsten is toxic for both people and animals as 5 μg kg^{-1} tungsten could cause death in animal embryo [5]. The mote containing tungsten may lead to emphysema and pulmonary

* Corresponding author.

fibrosis. 10–30 μg ml^{-1} of $Na_2WO_4/2H_2O$ could increase the probability of chromosomal reduplication during the lymphocytic culture. In addition, the toxicity of tungsten comes from its capability to interfere in molybdenum metabolism, therefore discouraging the enzymes biological activity containing molybdenum, phosphatase and adenosine triphosphate enzymes. Usually, tungsten exists in environmental water and soil samples as hexavalent, as WO_4^{2-} or all kinds of polyacid tungstate [5]. Due to the biological and toxic effects of this element on the people and animal, monitoring the concentration levels of tungsten in environmental samples becomes more important than ever before. The permissible concentration of tungsten in drinking water is 0.05 mg L^{-1} in Russia, and 15 mg L^{-1} in the USA, in the Commonwealth of Massachusetts [6]. However, most of the literature focuses on tungsten in alloys, minerals, rock, and ores [7–10], and little attention has been paid on tungsten in environmental water samples [11].

Nowadays, the removal of pollutants by adsorption is one of the most efficient techniques for environmental remediation, due to their simplicity, stability, and rareness of harmful byproducts, as well as both the adsorbent and the adsorbate being easily recyclable using appropriate desorption process [12]. Many adsorbents were used for the removal of aqueous tungsten such as pyroaurite-like anion exchangeable clay [13], novel Fe–Mg type hydrotalcite [14], synthetic zeolite [15], and Biopolymer coated clay particles [16], meanwhile the removal of rhodamine B dye was performed using different adsorbents such as MgO supported Fe–Co–Mn nanoparticles [17], Gel-like ZnO/Zr–MOF(bpy) nanocomposite [18], and functionalized locust bean pod (*Parkia biglobosa*) activated carbon [19].

Graphene nanosheets (GNS) are considered to be a new nanoadsorbent which are able to remove different pollutants including heavy metals, organic pollutants and pathogenic bacteria from aqueous environmental samples [20–26]. GNS are distinguishable by the high surface area and high adsorption ability due to the presence of negatively charged π electrons.

Rhodamine B (RhB) is an organic dye; chemical formula of $C_{28}H_{31}N_2O_3Cl$, has been widely used as an extraction reagent for the determination and removal of some negatively charged species through the formation of ion – association or complexes [27]. Rhodamine B in strongly acidic media occurs in cationic form, however, tungsten ions in this media occur in polytungstate anion form [28–30]. Therefore, rhodamine B could form ion – association complexes with polytungstate ions in acidic media. The aim of the present work will be concentrated on the removal process of tungsten ions and RhB dye from aqueous solutions and real water samples by using GNS. The morphology of GNS will be characterized with different chemical and physical techniques, and then modifying different experimental conditions on the extracting of tungsten ions and RhB dye from aqueous solution by GNS will be studied and optimized. Furthermore, the kinetic and thermodynamic characteristics of the adsorption procedure will be studied to understand the possible adsorption mechanism for the removal and spontaneity in order to increase the efficiency of the removal process. Finally, the application of the removal of tungsten ions and RhB dye from real water samples will be studied.

2. Experimental

2.1. Reagents and materials

All chemicals used in the present study were of high purity and quality so they would be employed without further purification. GNS were obtained from XG Science (xGnP® 300, USA) and were used as received. A stock of standard tungsten ions solution (1,000 mg L^{-1}) was prepared from sodium tungstate $Na_2WO_4{\cdot}2H_2O$ (Aldrich Chemical Co. Ltd., Milwaukee, WI, USA) by dissolving 0.1794 g of salt in 2% HNO_3 (100 mL), while a diluted standard tungstate sample solution (10 μg mL^{-1}) was prepared by diluting the stock solution with deionized water. The standard solution of rhodamine B (Sigma, St. Louis, MO, USA) with a concentration of 1×10^{-3} mol L^{-1} was prepared by dissolving an appropriate weight in deionized water (100 mL). A series solution of HCl/NaOH with pH (1–10) was applied on this method for removal of tungstate ions and rhodamine B dye by GNS.

2.2. Instruments

A Perkin-Elmer UV-visible spectrophotometer 190–1,100 nm (model Lambda 25, USA) with quartz cell (10 mm path width) was used to record all spectrophotometric measurements. Orion pH meter (model EA 940) was employed for recording pH measurements of the tested solutions. A digital micropipette (Volac, UK) and a digital sensitive balance (Citizen Scales Inc., USA) with four decimal numbers were used for preparing the standard solutions. The aqueous solutions were prepared by deionized water obtained from Milli-Q Plus system (Millipore, Bedford, MA, USA).

2.3. Characterization techniques

Scanning electron microscopy (SEM) image for the GNS was obtained using a Quanta 600 FEG SEM from FEI Company, USA. Nanostructure morphology of the GNS was measured using JEOL-JEM-1230 (USA) transmission electron microscopy (TEM). The GNS morphological structure and determining their thickness were characterized by scanning tunneling microscopy (STM), Agilent 5500 (USA). The X-ray diffraction (XRD) pattern of the GNS was collected on a Bruker DMAX 2500 (USA) X-ray diffractometer equipped with a Cu Kα radiation source (λ = 0.154 nm). The N2 adsorption–desorption isotherms for the GNS were conducted using a Micromeritics ASAP 2420 to determine the Brunauer–Emmett–Teller (BET) surface area.

2.4. Batch procedure used in the kinetic and thermodynamic studies

Aqueous solution (100 mL) containing tungsten ions (10 μg mL^{-1}) and RhB reagent (10^{-5} mol L^{-1} which equal 4.79 μg mL^{-1}) in the presence of drops of HCl (0.1 mol L^{-1}) to adjust pH at 1 was shaken with exactly weight (0.01 ± 0.001 g) from GNS for 1 h in a mechanical shaking water bath (JULABO SW23) with thermostatic control. Then, the aqueous phase was separated out by Millipore® filtration system with 10.0 μm membrane filter, and the amount of tungstate ions remained in the aqueous phase was determined spectrophotometrically by measuring the absorbance of the complex ion

associate formed between tungstate ions and RhB at 590 nm and the aid of an appropriate calibration curve. Finally, the adsorption percentage (%*E*) expressed as (Eq. (1)), and the amount of tungstate ions adsorbed (q_t) per unit mass of GNS (mg of WO_4^{-2} g^{-1}) expressed as (Eq. (2)), were calculated using the following equations:

$$\text{Adsorption}(\%E) = \frac{C_0 - C_t}{C_0} \times 100(\%) \quad (1)$$

$$q_t = \frac{(C_0 - C_t)V}{m} \quad (2)$$

where C_0 and C_t are the initial and final tungstate ions concentrations in solution (mg L^{-1}), respectively, V is the volume of the aqueous solution (L), and m is the mass of the GNS used (g).

2.5. Application

Three real water samples (tap water, sea water, and wastewater) were collected to estimate the efficiency of GNS for the removal of tungstate ions from environmental water solutions. Collection of sea water sample comes from the Red Sea in Jeddah city, KSA (Latitude deg. North 21.518333, Longitude deg. East 39.150677), the wastewater sample taken from the Membrane Bioreactor Technology WasteWater Treatment Plant (MBR 6000 STP) at King Abdulaziz University, Jeddah City KSA (Latitude deg. North 21.487954, Longitude deg. East 39.236748), and the sample of tap water was obtained from the lab in Department of Chemistry, King Abdulaziz University, Jeddah City, KSA (Latitude deg. North 21.497192, Longitude deg. East 39.249140). Then, the 0.45 μm cellulose membrane filter was used to filter the samples before being stored in 250 mL LDPE sample bottles in dark place at 5°C. A sample with volume 100 ml was treated as aforesaid in a batch step and the sample was shaken with GNS for 1 h time at 293 K temperature. The removal percentage of tungstate ions were determined spectrophotometrically, and the data were calculated as mentioned in the extraction batch step.

3. Results and discussions

3.1. Characterization of the nanographene

The physical properties of the GNS were explored using different characterization techniques; SEM, TEM, STM, XRD, and BET specific surface area analysis. It is clear from Figs. 1–3, that GNS present as transparent wrinkled overlapped sheets of different length and width, and with an average thickness of 20.0 nm. Fig. 4 shows XRD pattern of the GNS and the characteristic diffraction peaks at 2θ angles of 26.3°–54.1° similar to native graphite (JCPDS No. 12-0212), with hexagonal phase carbon with a space group of P63/mmc. The N_2 adsorption/desorption isotherms of the GNS at 77 K is presented in Fig. 5, and the BET specific surface area for the GNS was estimated and equaled to 279 m^2 g^{-1}. In addition, the adsorption/desorption isotherm of the GNS confirmed the presence of non-rigid aggregates of sheet-like

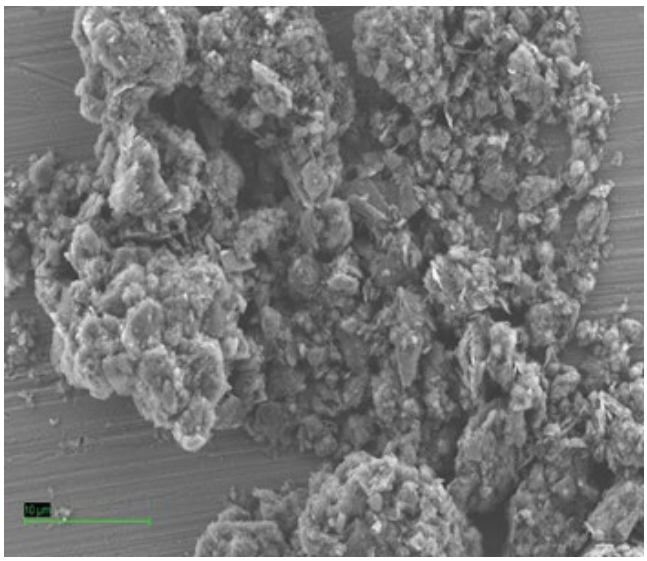

Fig. 1. Scanning electron microscopy image for GNS.

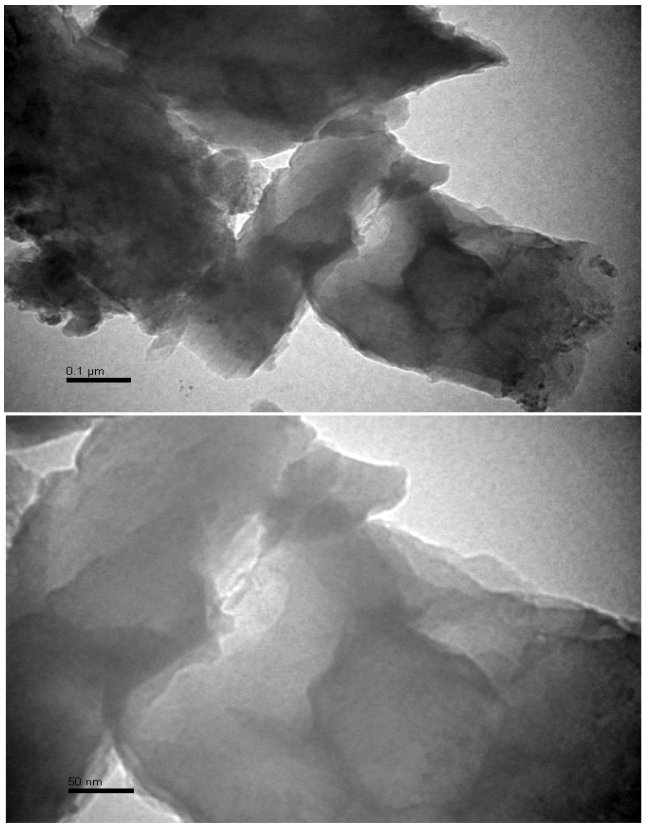

Fig. 2. Transmission electron microscopy image of GNS at different magnification powers.

graphene. Moreover, the adsorption-desorption isotherm could be classified as a type II isotherm with an H3 type hysteresis loop [31].

Preliminary study has shown that rhodamine B dye (RhB^+) in strongly acidic media exists in cationic form, while, tungsten (VI) ions in strongly acidic media exists

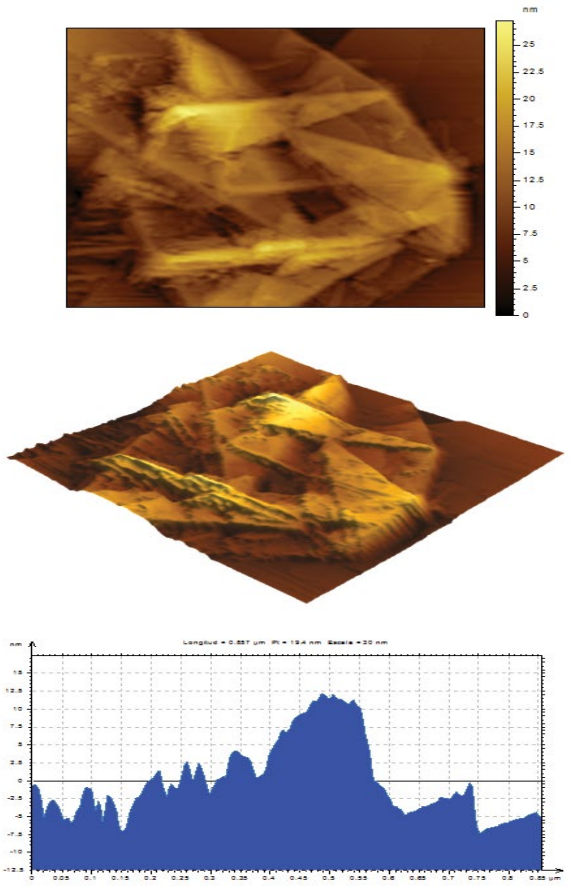

Fig. 3. Typical STM images of GNS (a) a topographic image, (b) 3-dimensional image, and (c) length-height scan image.

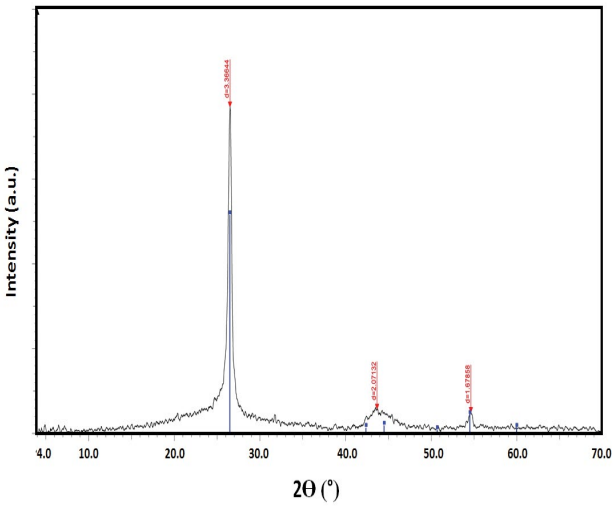

Fig. 4. XRD pattern of GNS.

in the form of polytungstate anion [28–30]. Therefore, rhodamine B can form ion – association complexes with polytungstate ions in acidic media. The formation of ion associate between tungsten (VI) ions and rhodamine B dye (RhB^+) in aqueous acidic solution of HCl was confirmed

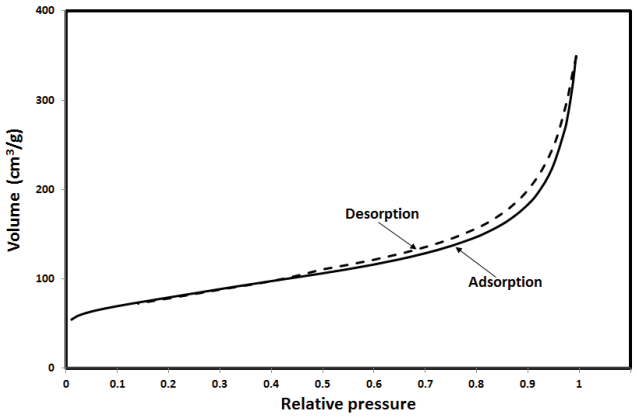

Fig. 5. Adsorption–desorption isotherms for GNS using nitrogen at 77 K.

by noticing of the color change of RhB dye from pink to purple colour after adding tungstate anion as shown in Fig. 6i, tube B. Also, the electronic spectrum of RhB dye (10^{-5} mol L^{-1}) in the aqueous solution showed one sharp absorption peak at 554 nm (Fig. 6ii, a), while this peak shifted from 554 to 590 nm after the addition of tungsten (VI) as shown in (Fig. 6ii, b), another indication for the ion associate formation. Otherwise, the structure of the formed ion associated between WO_4^{2-} ions and RhB in aqueous acidic (HCl) solution was confirmed by both of Job's continuous variation and molar ratio methods at λ_{max} of the ion associate (590 nm), and the result showed that the molar ratio was 1:2 (WO_4^{2-}: RhB^+). Subsequently, the proposed structure of the developed ion associated complex in aqueous acidic medium is $[(RhB^+)_2{\cdot}WO_4^{2}]$.

3.2. Adsorption study

The influence of aqueous phase pH on the sorption of [RhB-W(VI)] complex onto GNS was tested at various pH ranges 1–11 employing a mixture of HCl/NaOH. The results revealed that the maximum adsorption percentage was achieved at pH range 1–3, and this percentage was decreased dramatically by increasing the solution pH as illustrated in Fig. 7. This behaviour is referred to the presence of various species of W(VI) in aqueous solution counting on the variation of pH values wherever at pH less than 2, the $H_2W_{10}O_{40}^{6-}$ ion is in equilibrium state with $H_2W_6O_{20}^{2-}$ [32,33], so that, the strongly acidic media is suitable for both the formation and removal of the ion pair between RhB and W(VI) on GNS. In the following work, the pH of the aqueous solution was adjusted to pH 1 using a few drops of dilute HCl. Also, in low pH values, the surface of the GNS is mainly positive due to its coverage with the hydronium ions (H_3O^+), which greatly enhanced the electrostatic attraction with the negatively charged tungstate complex ions.

The effect of adsorbent mass is one of the important parameters in the removal and adsorption process, as it defines the adsorbent capacity for a specified initial concentration of the pollutant in a solution. The effect of the different mass of GNS dosage on the adsorption of tungstate ions (10 mg L^{-1}) from the aqueous solution was studied

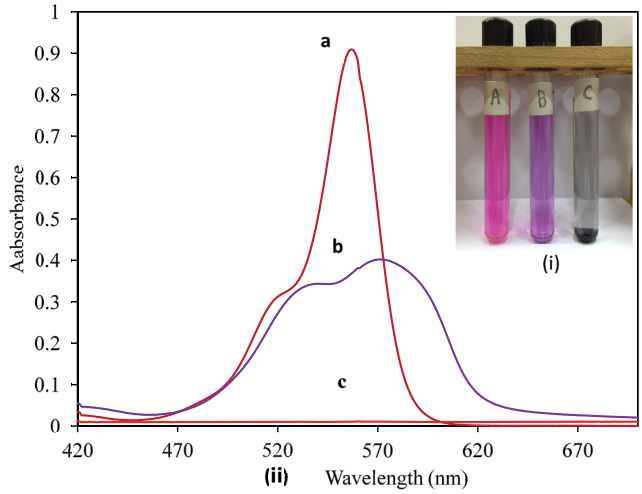

Fig. 6. (i) Photograph of RhB in aqueous phase in the absence of tungstate ions (A), and after adding 10 mg L^{-1} of tungstate ions (B) and after adding 0.01 g of GNS and shaking 60 min (C). (ii) Electronic spectra of RhB in aqueous phase in the absence of tungstate ions (a), and after adding 10 mg L^{-1} of tungstate ions with RhB (b) and after adding 0.01 g of GNS and shaking 60 min (c).

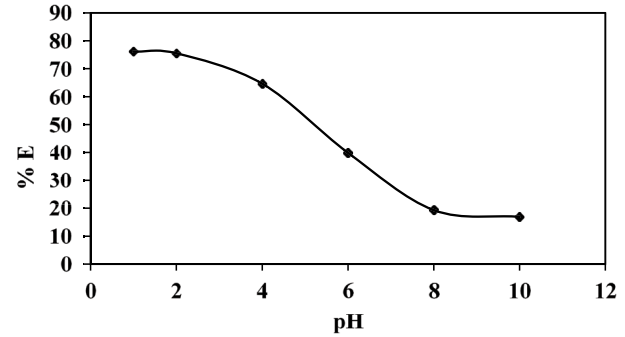

Fig. 7. Effect of pH solution on the adsorption of tungstate complex from aquatic solutions. Experimental conditions; RhB (10^{-5} M), W concentration 10 mg L^{-1}, graphene mass 0.01 g, shaking time 60 min, 100 mL solution volume, 293 K.

after shaking for 60 min and the results are shown in Fig. 8. The data from the figure showed that the percentage of the complex adsorbed in GNS increased gradually from 60.7% to 99.1% as GNS dose increased from 0.05 to 17.5 g L^{-1}, this is due to the higher doses providing more available surface areas of GNS and as a result, more active sites available for adsorption. In this work, we take a 10 g L^{-1} dosage of GNS, which agreed to 79% adsorption efficiency, to permit an evident observation of the other parameters influence.

The effect of shaking time between the adsorbate and the solid adsorbent played an important role in removing the pollutant species from aqueous solutions using adsorption process. Therefore, the effect of the shaking time on the removal process of tungstate complex ions by GNS was studied. The data in Fig. 9 shows as the shaking time increased, the adsorption process was gradually increased. This effect was chiefly observed in the first 20 min when

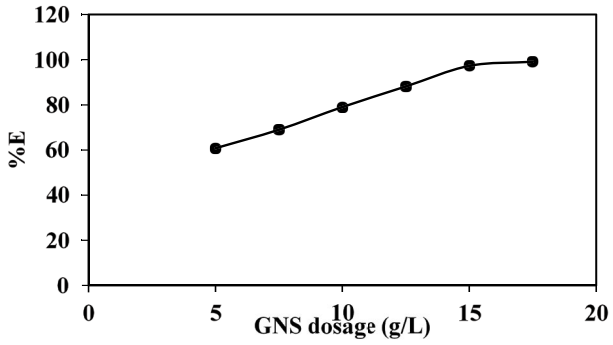

Fig. 8. Effect of GNS dosage on the adsorption of the tungstate complex from aquatic solutions by GNS. Experimental conditions; RhB (10^{-5} M), tungstate ions concentration 10 mg L^{-1}, pH = 1, volume solution 100 mL at 293 K.

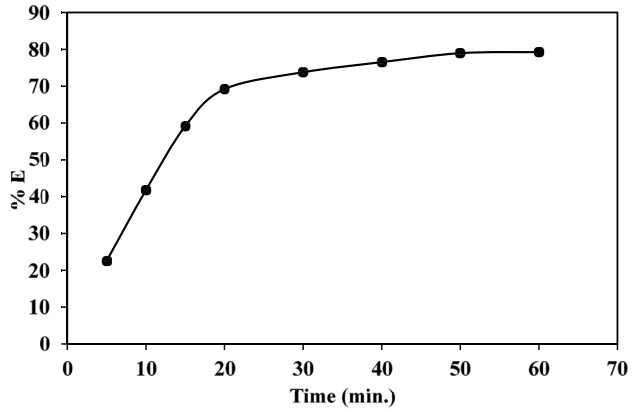

Fig. 9. Influence of shaking time on the removal of tungstate complex ions from aquatic solutions on GNS. Experimental conditions; RhB (10^{-5} M = 4.79 mg L^{-1}), tungstate concentration 10 mg L^{-1}, pH 1, GNS dosage 0.01 g L^{-1}, volume solution 100 mL at 293 K).

most $[(RhB^{+})_2 \cdot WO_4^{2-}]$ species were adsorbed, while adsorption of tungstate complex reached equilibrium during 50 min. This result refers to the adsorption of the complex ions on GNS occurring in two successive steps, the first and faster step, was the transfer of complex ions from the aqueous phase to the external surface of GNS. The second and slower step, was the diffusion of tungstate complex ions between the GNS bundles.

The solution temperature has a greater effect on the adsorption process as it greatly affects the diffusion/transfer of the adsorbate ions/molecules in solution. To determine the effect of the temperature solution on tungstate complex removal was studied at four various temperatures: 293, 303, 313, and 323 K at constant time. This has been noted with the raising of temperature solution from 293 to 303, 313, and 323 K was related with the increase in the efficiency of tungstate complex removed by GNS, which transformed from 79.3% to 84.8%, 92.7%, and 97.5%, respectively (Fig. 10). This data proposes the endothermic nature of the adsorption process, which will be discussed thoroughly in the thermodynamics study section.

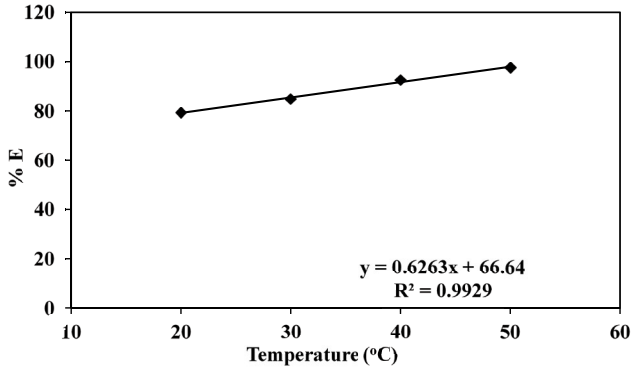

Fig. 10. Effect of the temperature solutions on the adsorption of tungstate complex ions from aquatic solutions by GNS. Experimental conditions; RhB (10^{-5} M), W concentration 10 mg L^{-1}, pH 1, GNS dosage 0.01 g L^{-1}, volume solution 100 mL).

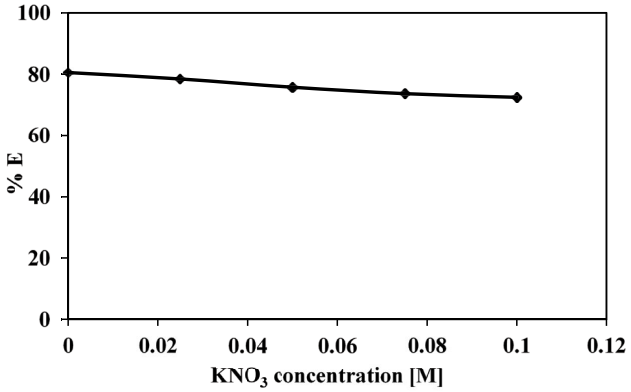

Fig. 11. Effect of KNO_3 concentration on the percentage of adsorption for tungstate complex from aquatic solutions onto GNS. Experimental conditions; RhB (10^{-5} M), W concentration 10 mg L^{-1}, pH 1, GNS dosage 0.01 g L^{-1}, volume solution 100 mL at 293 K.

The effect of ionic strength on the adsorption of metal ions in aqueous solution by solid adsorbent is critical because it can make various adsorption states by which electrostatic interactions between the surfaces of solid phase and the metal ions are either attractive or repellent. This effect was investigated, and the adsorption experiments were taking place by changing the ionic strength using KNO_3 concentrations of 0.025, 0.05, 0.075, and 0.1 mol L^{-1} (Fig. 11). The results showed that the percentage of adsorbed complex ions decreased gradually by increasing the ionic strength of the solution. This may be attributed to the fact that the presence of a cation such as K^+ decreases the interaction of the complex ions with the adsorbent surface due to the accumulation of charge about the adsorbent surface [33].

3.3. Kinetic behaviour for tungsten and rhodamine B dye adsorption onto nanographene

The kinetic adsorption of pollutants such as tungsten and rhodamine dye from aqueous solution by solid adsorbent such as GNS are important because it gives valuable insights on the reaction pathways and into the mechanism of sorption steps. From the effect of the shaking time, the result was corroborated by calculation of the half-life time ($t_{1/2}$) of tungstate complex sorption from the aqueous onto the GNS as a solid sorbents phase. The values of $t_{1/2}$ calculated from the plots of $\log C/C_0$ vs. time for tungstate complex sorption onto GNS and was found to be 1.6 ± 0.08 min in agreement with the values of $t_{1/2}$ reported earlier [34]. Thus, the kinetic of W and RhB sorption onto the GNS sorbent depends on the film and/or intra-particle diffusion where the slower one controls the overall rate of transport. The intra-particle diffusion for tungstate complex ions onto GNS sorbent was expressed by Weber–Morris model as the following [35].

$$q_t = K_{id}\left(t\right)^{1/2} + C \tag{3}$$

where q_t is the capacity of adsorption at whatever time (t), K_{id} is the diffusion of the intra- particle rate constant (mg g^{-1} $min^{-1/2}$), while C (mg g^{-1}) is a proportion constant for the thickness of the boundary layer. Stratifying the diffusion of intra-particle model to all the adsorption experimental data with zero intercept did not converge well and did not have straight lines pass through the origin and the value of K_{id} was equal 11.29 for tungsten and equal 5.42 for rhodamine B with the same correlation coefficient (R^2) 0.918 as is illustrated in Fig. 12a, which repudiate the suitability of the intra-particle diffusion model for all the experimental data. On the other hand, the plot of q_t vs. time was found linear at the initial stage of tungstate complex uptake by GNS sorbents up to 20 min and deviating on increasing the shaking time. Thus, the rate of retention step is film diffusion at the early stage of removal [36]. In this case the values of K_{id} can be studied from the two separate slopes of Weber–Morris curves (Fig. 12b), which were found equal to 18.77 and 3.3 mg g^{-1} for W ions and were equal to 9.01 and 1.58 mg g^{-1} for RhB, respectively with correlation coefficient R^2 equal 0.992 and 0.974, respectively.

The liquid film diffusion model can be confirmed mechanistically by the following [37]:

$$\ln\left(1-F\right) = -k_{fd} \times t \tag{4}$$

where F is the fractional attainment of equilibrium ($F = q_t/q_e$) and K_{fd} (min^{-1}) is the film diffusion rate coefficient. By drawing the plot between ln(1–F) and t with zero intercepts as presented in Fig. 13, the linear plot result proposes that the kinetics of this adsorption procedure was controlled by the diffusion of tungstate complex during the liquid film around the GNS.

Fractional power function kinetic model which is modified from Freundlich equation, and it can be illustrated by the following equation [38]:

$$\ln q_t = \ln a + b \ln t \tag{5}$$

where q_t (mg g^{-1}) is the adsorbed amount of tungstate complex ions per unit mass of GNS at any time t, while a and b are coefficients with $b < 1$. Applying the equation of fractional power function onto the data of experimental adsorption

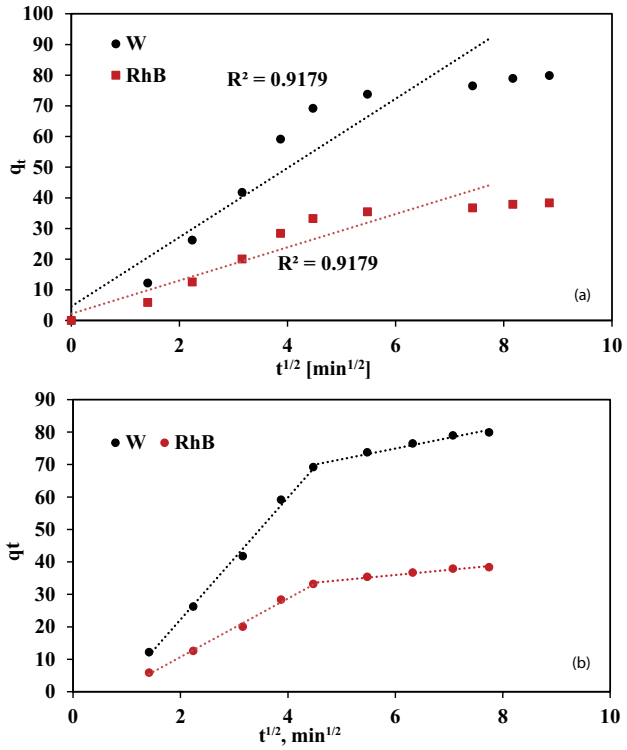

Fig. 12. Weber–Morris curve of tungstate complex adsorbed on GNS vs. square root of time. Experimental conditions process are aforesaid in the batch procedure step.

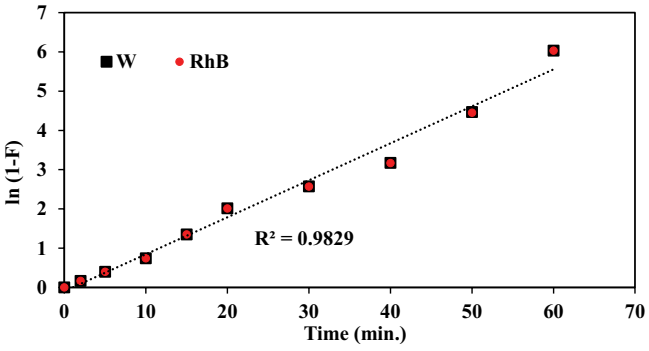

Fig. 13. Liquid film diffusion model plots of tungstate complex ions onto GNS.

process, the data did not come together well with low correlation coefficient (R^2) value of 0.923, as shown in Fig. 14. This shows the unsuitability of the fractional power function model for the description of tungstate complex ions adsorption by the GNS.

Lagergren pseudo-first-order model considered as one of the important equations that can be describe the rate of adsorption from an aqueous solution by the solid adsorbent. The Lagergren kinetic model can be illustrated by the following equation [39]:

$$\log\left(q_e - q_t\right) = \log q_e - \frac{K_1}{2.303}t \tag{6}$$

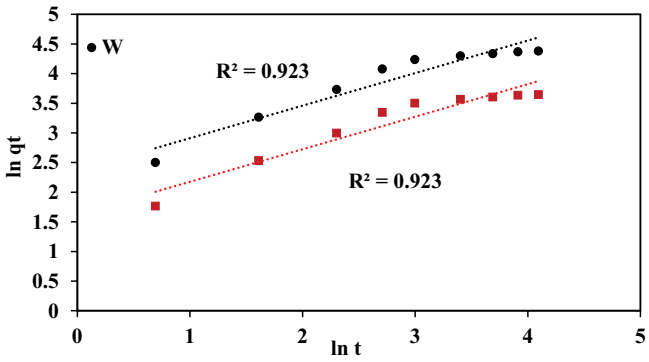

Fig. 14. Fractional power model plots of tungstate complex ions onto GNS.

where q_e and q_t are the values of the amount of tungsten complex adsorbed per unit mass of adsorbent GNS at equilibrium and at any time t, respectively and k_1 is the pseudo-first-order rate constant for the removal process. A linear plot between $\log(q_e - q_t)$ and time (t) was obtained as in (Fig. 15) and the calculated values of K_{Lager} and q_e were found equal to 0.104 min^{-1} and 95.19 mg g^{-1} respectively for W ions and were found 0.097 min^{-1} and 43.75 mg g^{-1} respectively for RhB species with correlation coefficient ($R^2 = 0.899$) for both plots. Furthermore, the calculated value of q_e was not nearly from the experimental value ($q_{e,\text{exp}}$). So that, the Lagergren pseudo-first-order kinetic model may not be appropriate to describe this process for removal of tungstate complex from aqueous solutions by GNS.

Pseudo-second-order model is another important equation in kinetics models because it is a special kind of Langmuir kinetics. A linearized model of pseudo-second-order can be illustrated by this equation [40]:

$$\frac{t}{q_t} = \frac{1}{k_2 q_e^2} + \frac{1}{q_e}t \tag{7}$$

where q_e and q_t are the amounts tungsten complex adsorbed as mentioned above, and k_2 (g mg^{-1} min^{-1}) is the pseudo-second-order rate coefficient. By plotting of t/q_t vs. t according to Eq. (7), the straight line with excellent R^2 value (0.992) was obtained as shown in (Fig. 16). Slope and intercept of the plot will be given values of (k_2) and (q_e) for tungstate complex which were found as 9.3×10^{-4} g mg^{-1} min^{-1} and 88.49 mg g^{-1}, respectively for W ions and were found equal to 2.2×10^{-3} g mg^{-1} min^{-1} and 41.84 mg g^{-1} for RhB species, respectively. This obtained data confirmed the suitability of the pseudo-second-order kinetic model to describe the adsorption of tungsten complex by GNS, which is consistent with previous studies [41,42].

Suitability of the pseudo-second-order kinetic model was tested by the equation of the Chi-square [43]:

$$\chi^2 = \sum \frac{\left(q_{e,\text{calc}} - q_{e,\text{exp}}\right)^2}{q_{e,\text{calc}}} \tag{8}$$

where $q_{e,\text{calc}}$ and $q_{e,\text{exp}}$ are the experimental and calculated amount of tungstate complex ions adsorbed at equilibrium

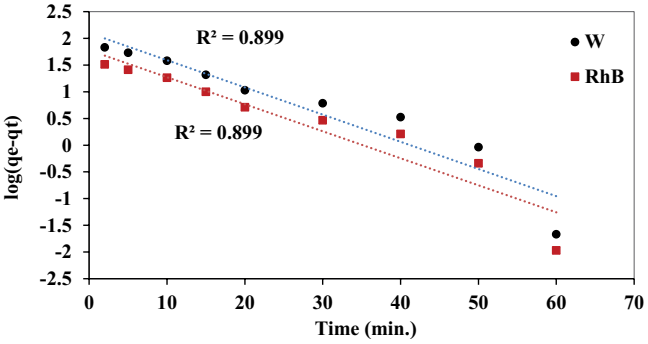

Fig. 15. Lagergren pseudo-first-order kinetic model plot of tungstate complex ions uptake on GNS.

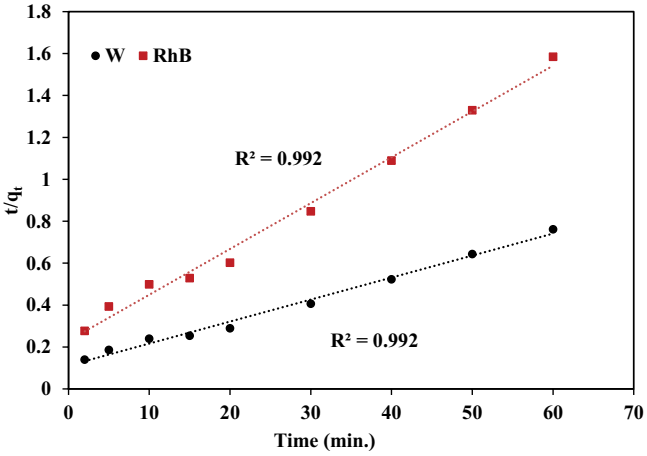

Fig. 16. Pseudo-second-order plot of tungstate complex ions removal by GNS.

per unit mass of GNS, respectively. According to the above results data comes from the kinetic models of the fractional power function model, the Lagergren pseudo-first-order model, the pseudo-second-order model and the Elovich model and depending on both the values of R^2 and the χ^2 for the Lagergren pseudo-first order, and pseudo-second-order kinetics models were (0.899, 2.46), and (0.992, 0.77), respectively for W ions and were found (0.899, 0.67), and (0.992, 0.29), respectively for RhB as shown in Table 1. This data confirms the suitability of the pseudo-second-order kinetic model for the description of tungstate complex ions adsorption by GNS.

Based on the above results, the mechanism of the removal of tungstate complex ions by GNS takes place in different steps, including the liquid film diffusion and the intra-particle diffusion, but they were not the rate determining steps. In addition, the removal process was best described by the pseudo-second-order kinetic model. Moreover, the removal process mainly is due to the π–π electron-donor acceptor interaction between the tungstate complex ions and the GNS surface.

A comparison of different adsorbents used for the removal of tungsten ions, and RhB was performed. According to the current proposed method, the maximum adsorption capacity obtained were 79.9 mg W g^{-1} GNS, and 38.35 mg RhB g^{-1}, whereas the maximum adsorption capacity obtained were 69.9 mg W g^{-1} of Mg-Fe-NO_3-LDH [13], 54.6 mg W g^{-1} of Fe-Mg type hydrotalcite [14], 44.90 mg W g^{-1} of synthetic zeolite [15], 23.9 mg W g^{-1} of biosorbent [16]. Meanwhile, in the case of RhB removal, the maximum adsorption capacity obtained were 2791mg RhB g^{-1} of MgO-FCM-NPs [17], 918.9 mg RhB g^{-1} of ZnO/Zr-MOF(bpy) [18], and 1111.1 mg RhB g^{-1} of activated carbon [19].

It is clear from the aforementioned comparison that the GNS is very competitive and promising adsorbent for the removal of tungsten ions, and RhB dye from aqueous solutions.

Table 1
Different kinetic models parameters for the adsorption of W ions and RhB on GNS at 293 K

	Intra-particle diffusion model			
	K_{id} (mg g^{-1} $min^{-1/2}$)	C (mg g^{-1})		R^2
W	11.29	4.599		0.918
RhB	5.42	2.21		0.918
	Liquid film diffusion model			
	K_{fd} (min^{-1})			R^2
W	0.096			0.981
RhB	0.096			0.981
	Fractional power kinetic model			
	a	b	ab	R^2
W	2.361	0.549	1.296	0.923
RhB	1.623	0.549	0.891	0.923
	Pseudo-first-order kinetic (Lagergren) model			
	$q_{e,exp}$ (mg g^{-1})	$q_{e,calc}$ (mg g^{-1})	k_1	R^2
W	79.90	95.19	0.104	0.899
RhB	38.35	43.75	0.097	0.899
	Pseudo-second-order kinetic model			
	$q_{e,exp}$ (mg g^{-1})	$q_{e,calc}$ (mg g^{-1})	k_2	R^2
W	79.90	88.49	9.3×10^{-4}	0.992
RhB	38.35	41.84	2.2×10^{-3}	0.992

3.4. Thermodynamic studies

The sorption of tungstate complex onto GNS was important to study thermodynamically at different temperature (293–323 K). The thermodynamic parameters, Gibbs free energy change (ΔG°), the enthalpy change (ΔH°) and entropy change (ΔS°) were calculated using the following equations:

$$K_c = \frac{C_{A^e}}{C_e} \tag{9}$$

$$\ln K_c = \frac{-\Delta H^\circ}{RT} + \frac{\Delta S^\circ}{R} \tag{10}$$

$$\Delta G^\circ = \Delta H^\circ - T\Delta S^\circ \quad (11)$$

$$\Delta G^\circ = -RT\ln K_C \quad (12)$$

where C_e is the equilibrium concentration of tungstate complex in aqueous solution (mg L^{-1}), C_A^e is the amount of tungstate complex adsorbed onto the GNS per liter at equilibrium (mg L^{-1}). T is the solution temperature by Kelvin, R is the gas constant (≈8.314 J K^{-1} mol^{-1}) and K_C is the equilibrium constant. The linear plot of ln K_C against 1,000/T for tungstate complex sorption onto GNS was shown in Fig. 17 over all the tested range of temperatures (293–323 K). The value of K_C increased as the solution temperature increases, and thus indicating that the adsorption of tungsten complex on GNS is an endothermic process. The values of ΔH°, ΔG°, and ΔS° were calculated from the plot to present in (Fig. 17) which found equal 61.13 ± 0.5 kJ mol^{-1}, –2.75 kJ mol^{-1} and 218 (J K^{-1} mol^{-1}), respectively at 293 K temperature.

The ΔH° value confirms the endothermic nature of the adsorption process. Increasing the solution temperature led to maximizing the interaction between the available active sites on the GNS surface and the tungsten complex. Therefore, the adsorption of tungstate complex increases. The positive value of ΔS° suggested the increase in the degree of freedom at the solid-liquid interface, mostly encountered in tungstate complex binding due to the release of water molecules of the hydration sphere during the adsorption processes. Generally, the negative value of ΔG°, and the positive values of ΔH° and ΔS°, indicated that the adsorption of tungsten complex on the GNS is a spontaneous entropy-driven process, endothermic nature process and physical in nature as the value of ΔG° was less than 40 kJ $mole^{-1}$ [44].

3.5. Environmental application

To study the applicability of GNS for removal of the tungsten complex from three real environmental samples (mentioned previously in the experimental section). The concentration of tungsten complex was studied for three samples, and the data were found to be under the detection limit of the UV–Vis measurement. So, the three samples were spiked with 10 mg L^{-1} concentration of tungsten ions, and were then shaken for 1 h at 293 K. The numerical percentages of tungsten complex removed from the real samples were found equal to 93.0% for Red Sea water, 94.8% for wastewater and 96.9% for tap water as shown in Fig. 18. Then, the GNS were collected and washed with acetone to remove the tungsten complex, dried, and reused for the removal tungsten complex again. Nearly the same percentage value of adsorption was gained for four cycles.

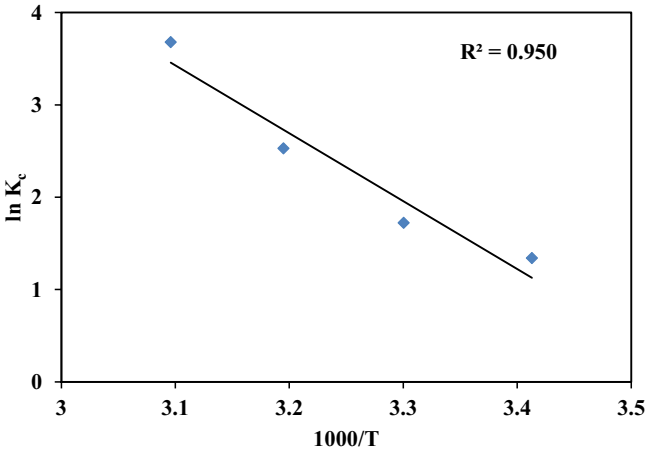

Fig. 17. Plot of ln K_C of tungstate complex removal on GNS against 1,000/T.

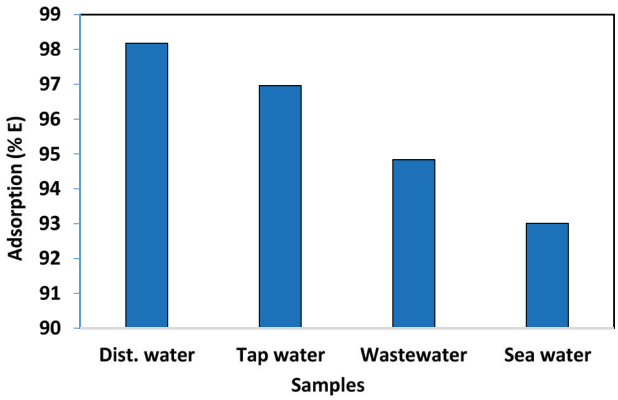

Fig. 18. Removal percentages of tungsten complex from three different real samples by GNS (Experimental conditions process: 100 ml volume solution, the pH = 1, 60 min shaking time, GNS dosage 0.02 g L^{-1}, 293 K temperature, and tungsten concentration 10 mg L^{-1}).

4. Conclusions

The removal of toxic tungsten ion (as tungstate) and rhodamine B dye from aqueous solutions by using GNS was studied. The SEM, TEM, STM, XRD, and BET specific surface area analyzer were used to characterize the GNS solid adsorbent, and the results displayed that GNS occur as plate-like overlapped transparent curling sheets of graphene with various dimensions, and characterized with BET specific surface area of 279 m^2 g^{-1}. The effects of varying experimental parameters that influence the removal/adsorption of tungsten ions from aqueous solution by GNS (such as pH, the mass of the GNS, contact time, solution temperature, and ionic strength) were examined. The results indicate that the efficiency of removal of a 10 mg L^{-1} of tungsten ions concentration on 17.5 mg mass of GNS per 100 mL in pH 1 within 60 min shaking time, and temperature at 293 K was equal to 99.1%. The kinetic of tungsten ions and rhodamine dye adsorption by GNS were carefully studied using various kinetic models, and the results exposed that the pseudo-second-order model was the most suitable model, which is characterized by both the biggest values of the correlation coefficient, and the lowest values of Chi-square. The thermodynamics study of the removal process showed that the adsorption process was spontaneous by increasing the solution temperature, endothermic nature with a positive value of entropy, and the interaction of the tungstate complex ions with the GNS was physical and electrostatic in nature. Finally, the efficiency of GNS was investigated by the removal of tungsten complex from three different real

environmental water samples. The results data displayed the excellent efficiency of the GNS for the removal of tungsten ions and rhodamine dye for four consecutive cycles.

Acknowledgment

This work was supported by the Deanship of Scientific Research (DSR), King Abdulaziz University, Jeddah, under grant No. (DF-447-130-1441). The authors, therefore, gratefully acknowledge DSR technical and financial support.

References

[1] R.L. Seiler, K.G. Stollenwerk, J.R. Garbarino, Factors controlling tungsten concentrations in ground water, Carson Desert, Nevada, Appl. Geochem., 20 (2005) 423–441.
[2] P.R. Sheppard, G. Ridenour, R.J. Speakman, M.L. Whitten, Elevated tungsten and cobalt in airborne particulates in Fallon, Nevada: possible implications for the childhood leukemia cluster, Appl. Geochem., 21 (2006) 152–165.
[3] A. Koutsospyros, W. Braida, C. Christodoulatos, D. Dermatas, N. Strigul, A review of tungsten: from environmental obscurity to scrutiny, J. Hazard. Mater., 136 (2006) 1–19.
[4] W.Q. Wang, Z.W. Zhao, Research advances of tungsten-molybdenum separation in tungsten extractive metallurgy, Chin. Tungs. Ind., 30 (2015) 49–55.
[5] G. Yiding, X. Gaoyang, S. Yuan, J. Songlin, Eds., Inorganic Chemistry Series, Vol. 8, Science Press, Peking, 1998, pp. 519–557.
[6] R. Lemus, C.F. Venezia, An update to the toxicological profile for water-soluble and sparingly soluble tungsten substances, Crit. Rev. Toxicol., 45 (2015) 388–411.
[7] L. Stefan, B. Slawomir, A new spectrophotometric method for the determination and simultaneous determination of tungsten and molybdenum in polyoxometalates and their Ln(III) complexes, J. Alloys Compd., 303–304 (2000) 132–136.
[8] T. Wang, Z. Ge, J. Wu, B. Li, A. Liang, Determination of tungsten in bulk drug substance and intermediates by ICP-AES and ICP-MS J. Pharm. Biomed. Anal. 19 (1999) 937–943.
[9] V. Padmasubashini, M.K. Ganguly, K. Satyanarayana, R.K. Malhotra, Determination of tungsten in niobium–tantalum, vanadium and molybdenum bearing geological samples using derivative spectrophotometry and ICP-AES, Talanta, 50 (1999) 669–676.
[10] N.K. Roy, A.K. Das, Determination of tungsten in rocks and minerals by chelate extraction and atomic-absorption spectrometry, Talanta, 33 (1986) 277–278.
[11] M.L. Firdaus, K. Norisuye, T. Sato, S. Urushihara, Y. Nakagawa, Y. Sohrin, Determination and distribution of Zr, Hf, Nb, Ta and W in the North Pacific Ocean, Geochim. Cosmochim. Acta, 70 (2006) 175–175.
[12] A. Dabrowski, Adsorption -from theory to practice, Adv. Colloid Interface Sci., 93 (2001) 135–224.
[13] L. Luo, Q. Guo, Y.Cao, Uptake of aqueous tungsten and molybdenum by a nitrate intercalated, pyroaurite-like anion exchangeable clay, Appl. Clay Sci., 180 (2019) 105179–105189.
[14] F. Ogata, T. Nakamura, E. Ueta, E. Nagahashi, Y. Kobayashi, N. Kawasaki, Adsorption of tungsten ion with a novel Fe-Mg type hydrotalcite prepared at different Mg^{2+}/Fe^{3+} ratios, J. Environ. Chem. Eng., 5 (2017) 3083–3090.
[15] F. Ogata, Y. Iwata, N. Kawasaki, Properties of novel adsorbent produced by hydrothermal treatment of waste fly ash in alkaline solution and its capability for adsorption of tungsten from aqueous solution, J. Environ. Chem. Eng., 3 (2015) 333–338.
[16] H. Gecol, P. Miakatsindila, E. Ergican, S. R. Hiibel, Biopolymer coated clay particles for the adsorption of tungsten from water, Desalination, 197 (2006) 165–178.
[17] S. Rahdar, A. Rahdar, M.N. Zafar, S.S. Shafqat, S. Ahmadi, Synthesis and characterization of MgO supported Fe–Co–Mn nanoparticles with exceptionally high adsorption capacity for Rhodamine B dye, J. Mater. Res. Technol., 8 (2019) 3800–3810.
[18] W. Cui, X. Kang, X. Zhang, X. Cui, Gel-like ZnO/Zr-MOF(bpy) nanocomposite for highly efficient adsorption of Rhodamine B dye from aqueous solution, J. Phys. Chem. Solids, 134 (2019) 165–175.
[19] O.S. Bello, K.A. Adegoke, O.O. Sarumi, O.S. Lameed, Functionalized locust bean pod (*Parkia biglobosa*) activated carbon for Rhodamine B dye removal, Heliyon, 5 (2019) e02323.
[20] M. Abdel-Salam, L.A. Al-khateeb, M.A. Abdel-Fadeel, Removal of toxic ammonium ions from water using nanographene sheets, Desal. Water Treat., 129 (2018) 168–176.
[21] M. Abdel-Salam, Adsorption of nitroaniline onto high surface area nanographene, J. Ind. Eng. Chem., 28 (2015) 67–72.
[23] L.A. Al-Khateeb, W. Hakami, M. Abdel Salam, Removal of non-steroidal anti-inflammatory drugs from water using high surface area nanographene: kinetic and thermodynamic studies, J. Mol. Liq., 241 (2017) 733–741.
[24] N.M. Mahmoodi, M. Oveisi, M. Bakhtiari, B. Hayati, A.A. Shekarchic, A. Bagherid, S. Rahimi, Environmentally friendly ultrasound-assisted synthesis of magnetic zeolitic imidazolate framework - graphene oxide nanocomposites and pollutant removal from water, J. Mol. Liq., 282 (2019) 115–130.
[25] S.A. Hosseini, Z. Shokri, S. Karami, Adsorption of Cu(II) to mGO@Urea and its application for the catalytic reduction of 4-NP, J. Ind. Eng. Chem., 75 (2019) 52–60.
[26] A.I. Abd-Elhamid, E.A. Kamoun, A.A. El-Shanshory, H.M.A. Soliman, H.F. Aly, Evaluation of graphene oxide-activated carbon as effective composite adsorbent toward the removal of cationic dyes: composite preparation, characterization and adsorption parameters, J. Mol. Liq., 279 (2019) 530–539.
[27] H.M. Al-Saidi, A.A. Bindary, A.Z. El-Sonbati, M.A. Abdel-Fadeel, Fluorescence enhancement of rhodamine B as a tool for the determination of trace and ultra-trace concentrations of bismuth using dispersive liquid–liquid microextraction, RSC Adv., 6 (2016) 21210–21218.
[28] A. Corsini, K.S. Subramanian, Studies on tungstate solutions in acid medium, J. Inorg. Nucl. Chem., 40 (1978) 1777–1779.
[29] P. Ning, H. Caoa, Y. Zhang, Selective extraction and deep removal of tungsten from sodium molybdate solution by primary amine N1923, Sep. Purif. Technol., 70 (2009) 27–33.
[30] J.L. Zhang, Z.W. Zhao, X.Y. Chen, X.H. Liu, Thermodynamic analysis for separation of tungsten and molybdenum in W-Mo-H_2O system, Chin. J. Nonferrous Met., 23 (2013) 1463–1470.
[31] M. Thommes, K. Kaneko, A.V. Neimark, J.P. Olivier, F. Rodriguez-Reinoso, J. Rouquerol, K.S.W. Sing, Physisorption of gases, with special reference to the evaluation of surface area and pore size distribution (IUPAC Technical Report), Pure Appl. Chem., 87 (2015) 1051–1069.
[32] S. Li, N. Deng, F. Zheng, Y. Huang, Spectrophotometric determination of tungsten(VI) enriched by nanometer-size titanium dioxide in water and sediment, Talanta, 60 (2003) 1097–1104.
[33] S.A. Dastgheib, D.A. Rockstraw, A systematic study and proposed model of the adsorption of binary metal ion solutes in aqueous solution onto activated carbon produced from pecan shells, Carbon, 40 (2002) 1853–1861.
[34] S. Palagyi, T. Braun, Separation and Pre-concentration of Trace Elements and Inorganic Species on Solid Polyurethane Foam Sorbents, Z.B. Alfassi, C.M. Wai, Eds., Preconcentration Techniques for Trace Elements, CRC Press, Boca Raton, FL, 1992.
[35] W.J. Weber, J.C. Morris, Kinetics of adsorption on carbon from solution, J. Sanit. Eng. Div. Am. Soc. Civ. Eng., 89 (1963) 31–36.
[36] A.K. Bhattacharya, C. Venkobachar, Removal of cadmium (II) by low cost adsorbents, J. Environ. Eng., 110 (1984) 1–29.
[37] G.E. Boyd, A.W. Adamson, L.S. Myers, The exchange adsorption of ions from aqueous solutions by organic zeolites II kinetics, J. Am. Chem. Soc., 69 (1947) 2836–2848.
[38] R.C. Dalal, Desorption of soil phosphate by anion-exchange resin, Commun. Soil Sci. Plant Anal., 5 (1974) 531–538.

[39] S. Lagergren, About the theory of so-called adsorption of soluble substances, Zur theorie der sogenannten adsorption gel Ster stoffe, Kungliga Svenska Vetenskapsakademiens, Handlingar, Band, 24 (1898) 1–39.
[40] W. Rudzinski, W. Plazinski, On the applicability of the pseudo-second-order equation to represent the kinetics of adsorption at solid/solution interfaces: a theoretical analysis based on the statistical rate theory, Adsorption, 15 (2009) 181–192.
[41] R. Foroutan, H. Esmaeili, A.M. Sanati, M. Ahmadi, B. Ramavandi, Adsorptive removal of Pb (II), Ni (II), and Cd (II) from aqueous media and leather wastewater using *Padinasanctae-crucis* biomass, Desal. Water Treat., 135 (2018) 236–246.
[42] H. Esmaeili, R. Foroutan, Adsorptive behavior of methylene blue onto sawdust of sour lemon, date palm, and eucalyptus as agricultural wastes, J. Dispersion Sci. Technol., 40 (2019) 990–999.
[43] V. Bagdonavicius, M.S. Nikulin, Chi-square goodness-of-fit test for right censored data, Int. J. Appl. Math. Stat., 24 (2011) 30–50.
[44] H. Nollet, M. Roels, P. Lutgen, P.V. der-Meeren, W. Verstraete, Removal of PCBs from wastewater using fly ash, Chemosphere, 53 (2003) 655–665.